European Journal of Pharmaceutics and Biopharmaceutics 212 (2025) 114728

Contents lists available at ScienceDirect

European Journal of Pharmaceutics and Biopharmaceutics

journal homepage: www.elsevier.com/locate/ejpb

Research paper

# Enhanced ex vivo skin retention of bicalutamide using a nano-in-micro composite: Drug-loaded lipid vesicles in a dissolving microarray patch

Miquel Martínez-Navarrete [a], Mafalda Correia [b,c], J.Alejandro Bernabeu-Martínez [a], Ana Cláudia Paiva-Santos [b,c], Ana Borrego-Sánchez [a], Antonio José Guillot [a,*]

[a] Department of Pharmacy and Pharmaceutical Technology and Parasitology, University of Valencia, Avenue Vicent Andrés Estelles s/n. Spain. Valencia, Burjassot 46100, Spain
[b] Department of Pharmaceutical Technology, Faculty of Pharmacy of the University of Coimbra, University of Coimbra, Azinhaga de Santa Comba, 3000-548 Coimbra, Portugal
[c] REQUIMTE/LAQV, Group of Pharmaceutical Technology, Faculty of Pharmacy of University of Coimbra, University of Coimbra, 3000-548 Coimbra, Portugal

ARTICLE INFO

*Keywords:*
Bicalutamide
Dissolving Microneedles
Lipid Vesicles
Local Skin Delivery
Androgenetic Alopecia

ABSTRACT

Antiandrogens are a family of drugs that block the biological effects of androgens, which are commonly used to treat a plethora of androgen-dependent conditions. However, their effectiveness highly depends on treatment compliance and their use is not exempt from side effects. Bicalutamide (BIC) is a testosterone blocker that, due to its peripheral tissue selectivity, offers the advantage of fewer side effects compared to other antiandrogens such as finasteride or dutasteride. In this study, BIC-loaded lipid vesicles (LVs) were developed and incorporated into a PVP/PVA-based Dissolving Microarray Patches (BIC-LVs@DMAPs) for BIC skin local delivery. First, the mechanical and insertion properties of the BIC-LVs@DMAPs were assessed. Then, the *in vitro* biocompatibility of the formulation was determined in keratinocytes. Finally, the effectiveness of the formulation to deliver BIC through skin was explored *ex vivo* using murine skin. BIC-LVs@DMAPs exhibited optimal mechanical and insertion properties to effectively perforate the *stratum corneum* and facilitate the passage of BIC-LVs. *Ex vivo* studies demonstrated the efficacy of BIC-LVs@DMAPs to improve the skin retention of BIC, while *in vitro* cytotoxicity results ensured their safety profile. Overall, these results pave the way for further *in vivo* studies and clinical application to improve the current early stages androgenetic alopecia topical treatments.

## 1. Introduction

Antiandrogens, also known as androgen antagonists, are a group of drugs that block the biological effects of androgens like testosterone and dihydrotestosterone. Particularly, their action mechanisms rely on the androgen receptor blockade and the inhibition or suppression of androgen production. Therefore, antiandrogens are used to treat several androgen-dependent conditions. In men, they are widely used for the treatment of scalp hair loss, prostate cancer, benign prostatic hyperplasia, and precocious puberty [1–3]. Acne, seborrhea, scalp hair loss and polycystic ovary syndrome (PCOS) are the main conditions treated in women with this type of drugs [4–7]. Their side effects depend on the type of antiandrogen and the received drug dose. Particularly, long-term antiandrogen therapies are associated with sexual dysfunction, bone fractures, elevated risk of cardiac disorders, and depression in the male population, among other effects [8,9]. Although antiandrogens are generally better tolerated in women, they can cause menstrual irregularities, osteoporosis, and hot flashes due to the suppression of androgen production, as androgens can be converted into estrogens [10].

The development of new and better drugs and formulations to treat these conditions with fewer adverse effects is an urgent need because of their high incidence and patients' demands. For example, a total of 1,414,259 new cases and 375,304 deaths related to prostatic cancer were reported worldwide in 2020 [11]. PCOS affects between 4–20 % of women at reproductive age, depending on the diagnostic criteria [12]. Although androgenetic alopecia is the most common type of progressive hair loss disorder in men, affecting 50 % by the age of 50 years[13], a non-negligible proportion of women are also affected. This condition can have a considerable negative impact on emotional regulation, self-confidence, and feelings of stigmatization [14]. Several FDA-approved antiandrogen medications are currently available, i.e., apalutamide (Erleada®), darolutamide (Nubeqa®), enzalutamide (Xtandi®),

* Corresponding author.
*E-mail address:* antonio.guillot@uv.es (A.J. Guillot).

https://doi.org/10.1016/j.ejpb.2025.114728
Received 5 February 2025; Received in revised form 7 April 2025; Accepted 26 April 2025
Available online 27 April 2025

flutamide (Eulexin®), nilutamide (Nilandron®), and bicalutamide (Casodex®) [15].

In this study, Bicalutamide (BIC) which belongs to the testosterone blocker drug group and has been regularly used to stop the growth and spread of cancerous cells in prostatic cancer cases [16], was selected for developing a novel healthcare device. Similar to finasteride (Propecia®) or dutasteride (Avodart®), which were repurposed for the treatment of androgenetic alopecia following serendipitous findings [17], BIC also holds potential for the treatment of androgenetic alopecia. Currently, the BIC dose orally administered to treat hair loss conditions is 25 mg per day [18]. On this matter, unlike 5-α reductase inhibitors, BIC does not inhibit this enzyme and solely blocks the binding of testosterone and dihydrotestosterone to their receptors [19]. The mechanism of BIC offers the advantage of producing fewer side effects compared to other anti-androgens due to its peripheral tissue selectivity [20]. Local administration of these drugs can also reduce the appearance of systemic side effects when treating skin conditions. However, it has been considered that only molecules with low molecular weight (<500 Da) [23], intermediate partition coefficient and low degree of ionization can be effectively absorbed after topical application [24]. To overcome these limitations, advanced drug delivery systems have been developed over the past decades. Among them, Microarray Patches (MAPs) are devices with microscopic needle-like projections that perforate the outer epidermal skin layer, also known as the *stratum corneum*, which performs the barrier function against the entrance of exogenous substances to the body. The created microchannels enhance the passage of large molecules and supramolecular entities that present unfavorable physicochemical properties to diffuse passively through the skin structure [21]. Due to the length of microneedles (100–500 μm), MAPs can penetrate the *stratum corneum* layer (40–50 μm) reaching the epidermal and superficial dermal structures, where the skin microvascularized environment is located, without touching the skin nerve endings situated in the deeper dermis layers [22]. Thus, they stand out for being a pain-free strategy. Other advantages attributed to MAPs as a dermal or transdermal approach over oral dosage forms include improved patient adherence and treatment compliance [23], and avoidance of certain obstacles that lead to impaired bioavailability, such as the first-passage effect [24], drug hydrolysis by gastric pH [25], drug complexation with bile acids or food components, and malabsorption features after digestive surgeries or because of intestinal diseases [26,27]. In contrast to parenteral routes, MAPs offer a comfortable alternative for patients. First, several MAPs prototypes are self-administrable devices that do not require to be administered by medical personnel [28]. Second, because of their small size, inconspicuous profile, and ability to be incorporated into band-aid-like patches, MAPs can be aesthetically pleasing for patients and further reduce the perception of pain and anxiety [29], particularly for individuals with needle phobia, who comprise approximately 20 % of the population [30].

Since their conception, different MAPs prototypes have been developed, i.e., solid, hollow, coated, dissolving, swelling, hydrogel-forming, etc. Specifically, Dissolving Microarray Patches (DMAPs) are made with different biodegradable materials in which the drugs are loaded. Water-soluble polymers like polyvinyl alcohol (PVA) [31], polyvinyl pyrrolidone (PVP) [32], poly (methyl vinyl ether-alt-maleic acid) (PMVE-MA) [33], or hyaluronic acid (HA) [34], are often used for DMAP preparation in order to avoid organic solvent use, thus, reducing the potential toxicity of the final formulation and making its production more eco-friendly [35]. Approaches based on the use of DMAPs and swelling microneedles are more compatible with small and hydrophilic molecules due to their easy incorporation in these devices [36]. However, it is also possible to formulate them with hydrophobic drugs through the use of solubilizing agents or intermediate nanocarriers [37]. The strategy used with DMAPs is defined as "*poke and release*" approach. Particularly, it involves the polymer dissolution after DMAPs insertion and contact with the interstitial skin fluids, which subsequently triggers cargo release [38]. In addition, the use of different polymers, proportions and concentrations consequently allows for modulation of the release process and drug absorption [39]. Because of the limited cargo that DMAPs can host in the needle-like projections, they are commonly used for local skin delivery of active substances without achieving a systemic absorption.

The aim of this study is to develop a DMAPs-based strategy to deliver BIC locally within the skin structure to offer a new healthcare device for the early-stage treatment of either male or female androgenetic alopecia, where the areas with miniaturized hair can be covered by BIC-LVs@DMAPs devices. As mentioned above, the lipophilicity of BIC limits its incorporation into the hydrophilic PVA/PVP matrix. To overcome this issue, different systems have been suggested to incorporate hydrophobic drugs in DMAPs as an intermediate water-dispersible formulation, i.e., nanosuspensions, nanocrystals and nanoparticles [37]. In this case, we suggest ultra-flexible lipid vesicles (LVs) to allow the incorporation of BIC inside the hydrophilic polymeric network (BIC-LVs@DMAPs) [40]. BIC-LVs were characterized in terms of size, polydispersity index (PDI), surface charge, and biocompatibility in a keratinocyte cell line. Moreover, after incorporating them in DMAPs, the mechanical strength, insertion properties, drug release, and cellular biocompatibility of PVA-PVP-based DMAPs loaded with BIC-LVs were also studied. Finally, *ex vivo* BIC absorption and skin drug retention obtained from BIC-LVs@DMAPs were determined in a surrogate model to investigate the efficiency and performance of the developed system.

## 2. Materials and Methods

### 2.1. Materials

Phospholipon 90G® −soybean phosphatidylcholine- (P90G) was purchased from Lipoid (Steinhausen, Switzerland). Polysorbate 80 (Tween 80®) was acquired from Scharlab (Sentmenat, Spain). Sodium dodecyl sulphate was obtained from Sigma-Aldrich (St. Louis, USA). Lactose and sorbitol were purchased from Guinama (Valencia, Spain). PVA (MW 9–10 kDa) and PVP (MW 40 kDa) were purchased from Sigma-Aldrich (St. Louis, USA). Polydimethyl siloxane microneedle molds (PDMS) (15x15 microneedles, height 600 μm, base 200 μm) were acquired from Micropoint Technologies (Singapore). Dimethyl sulfoxide (DMSO) and 3-[4,5-dimethylthiazol-2-yl]-2,5-diphenil-tetrazolium bromide (MTT) were purchased from Sigma-Aldrich (St. Louis, USA). Dulbecco's modified eagle medium (DMEM) was obtained from Thermo Fisher Scientific (Waltham, USA). Phosphate salts ($KH_2PO_4$ and $Na_2HPO_4$), NaCl and KCl were purchased from Scharlab (Sentmenat, Spain). Cosmetic ethanol and propylene glycol were purchased from Guinama (Valencia, Spain). HPLC-grade water was obtained by Milli-Q purification (Millipore Corporation; USA) with resistance >18 MΩ cm, and total organic carbon (TOC) < 10 ppb. HPLC-grade methanol and acetonitrile were purchased from VWR International (Radnor, USA).

### 2.2. Preparation of BIC-LVs

BIC-LVs were prepared by the Bangham's method as described elsewhere [41,42]. Briefly, P90G (60 mM), Tween 80® (5 mM) and BIC (4.5 mM) were dissolved in methanol, which was removed after using a rotary evaporator (BUCHI R-210; Büchi) under stirring at 50 °C (100 mBar pressure) and left under vacuum overnight to remove any organic solvent traces. The obtained lipid thin-film was hydrated by addition of PBS pH 7.4 (10 mL) and stirred at 55 °C for 1 h. To reduce the BIC-LVs size, the obtained multi-lamellar BIC-LVs dispersion was sonicated for 2 h at 37 kHz (Elma S30 H; Elmasonics) and cooled down to 4 °C. Then, it was extruded (20 times) through a 200 μm pore-size polycarbonate membrane (LiposFast-Basic Extruder; Avestin). Finally, free-BIC was removed from the BIC-entrapped fraction by dialysis purification in Phosphate buffer pH 7.4 (2 L) at 4 °C (Spectra/Por® molecular porous membrane tubing, 14 MWCO; Repligen). Unloaded LVs (Blank-LVs) were synthesized using the same methodology.

### 2.3. BIC-LVs morphology study

The morphology of the BIC-LVs was observed by TEM imaging (HT7800; Hitachi). For this, BIC-LVs were stained using an adaptation of Théry *et al.* method. Briefly, BIC-LVs (1:100 dilution) were fixed in paraformaldehyde 2 % (w/v) for 30 min. Afterwards, they were deposited on a carbon grid for 15 min. Finally, samples were washed twice, fixed in glutaraldehyde 1 % (w/v), and contrasted with uranyl acetate 1 % (w/v) and methylcellulose 0.5 % (w/v) [43].

### 2.4. Determination of entrapment efficiency of BIC-LVs

Entrapment efficiency (EE) was determined directly by calculating the amount of BIC encapsulated in lipid vesicle dispersions using Eq. (1) [44].

$$EE(\%) = \frac{Qe}{Qt} \cdot 100 \quad (1)$$

where Qe is the amount of BIC encapsulated, and Qt is the amount of BIC used for each batch preparation. For this, 0.5 mL of LVs dispersion was incubated for 1 h with a lysis medium containing sodium dodecyl sulphate 1 % (w/v) (1:9 proportion) to dissolve all the vesicle components [45–47]. The final mixture was centrifuged and filtered prior to BIC content analysis using the analytical method described in Section 2.14. The reported results were obtained as an average of three different batches (n = 3).

### 2.5. Determination of lipid vesicle size, polydispersity index and surface charge

Dynamic Laser Scattering (DLS) was used to measure the particle size and polydispersity index (PDI) [48,49], whereas zeta potential was determined by Laser Doppler Electrophoresis (LDE) (Malvern nanozetasizer; Malvern Panalytical) [50]. All measurements were conducted at room temperature and a measurement angle of 173°. Each sample was diluted KCl 1 mM (1:1000) and analyzed in triplicate. The reported results were obtained as an average of three different batches (n = 3).

### 2.6. Determination of phospholipid content of BIC-LVs

Phosphatidylcholine incorporated into the LVs was determined by Rouser's method [51]. Briefly, 100 μl of the liposomal dispersion was heated at 270 °C until complete liquid evaporation. Then, 450 μL of perchloric acid 70 % (v/v) was added, and the mixture was heated to 250 °C for 30 min. After cooling down, 3.5 mL of water, 500 μL of ammonium molybdate 2.5 % (w/v), and 500 μL of ascorbic acid 10 % (w/v) were added. The resulting mixture was vortexed and incubated at 100 °C for 7 min. After cooling down, the absorbance was measured at 820 nm (spectrophotometer U-2900; Hitachi-Hightech). Phospholipid recovery was quantified using a calibration curve within the range of 0.4–450 mg of PC (Eq. (2), demonstrating optimal linearity ($r^2 = 0.941$). The reported results were obtained as an average of three different batches (n = 3).

$$y = 0.4735x + 0.0272 \quad (2)$$

### 2.7. Freeze-drying of BIC-LVs

For preservation purposes after their preparation, LVs were freeze-dried using lactose and sorbitol as cryoprotective agents. Lactose solution was prepared at a molar ratio P90G/sugar 1:10, while sorbitol was used at a 2.5 % (v/v) concentration [52,53]. For this, 100 μL of sample were placed together with 400 μL of cryoprotective agent in glass vials. Samples were frozen at −80 °C for 24 h and freeze-dried for 48 h using a freeze-dryer at −50 °C and 0.08 mbar (LyoQuest HT-40; Telstar). To guarantee the quality of the freeze-dried product, residual water content was determined by thermogravimetric analysis (TGA) (SDTA 851e; Mettler Toledo). Temperature scans were performed from 25 to 200 °C at a scan rate of 10 °C/min [54]. Changes in size, PDI, zeta potential, and EE after freeze-drying of BIC-LVs and subsequent reconstitution were evaluated (n = 3).

### 2.8. Preparation of BIC-LVs@DMAPs

DMAPs containing BIC-LVs were prepared as described elsewhere [55,56]. First, PVA and PVP polymers were dissolved in water to create stock blends, which were then used to prepare gels at the desired polymer concentrations. These gels were mixed with reconstituted freeze-dried BIC-LVs (5 % w/v) until homogeneous. The final polymer concentrations were 15 % (w/v) for PVA and 5 % (w/v) for PVP. The resulting gel was then poured into PDMS microneedle molds (0.25 g), and then a pressure of 3–4 bar was applied (Protima® pressure tank, TÜV Rheinland, Germany) for 45 min to ensure proper mold cavity filling. Finally, DMAPs were dried at room temperature for 24–48 h and peeled off from the molds. To guarantee complete water drying, the residual water content was determined by TGA (SDTA 851e; Mettler Toledo) after preparation and 2-months of storage in a dry-seal desiccator. Temperature scans were performed from 25 to 200 °C at a scan rate of 10 °C/min [57].

### 2.9. BIC-LVs@DMAPs morphology

The morphology of the BIC-LVs@DMAPs was observed by SEM imaging (SCIOS 2 FIB; Thermo Scientific). For this, BIC-LVs@DMAPs were coated with a conductive gold:paladium layer. Images were taken using a voltage and current of 3 kV and 0.2nA, respectively [58].

### 2.10. BIC-LVs@DMAPs mechanical strength and insertion properties

Mechanical strength of DMAPs containing BIC-LVs was evaluated using a TA-TX plus Texture Analyzer (Stable Microsystem; UK). DMAPs were visualized before testing using a light microscope (Leica ICC50 HD; Leica Microsystems) and then carefully placed on the flat plate with the needles facing downwards. The compression mode was applied with a force of 32 N/m for 30 s to compress the DMAPs against a stainless-steel surface. Finally, DMAPs were observed under the light microscope to compare the decrease in needles length [59]. The insertion depth of DMAPs was determined using an artificial skin model. The setup and conditions were similar to those used in mechanical strength studies but pressing the DMAPs against eight sequential Parafilm M® layers instead of the stainless flat surface. The holes created in each layer were counted using a light microscope to evaluate the insertion performance [60]. The reported results were obtained as an average of three different replicates (n = 3).

### 2.11. In vitro release study of BIC-LVs@DMAPs and kinetic modelling fitting

*In vitro* release studies were carried out by dissolving the BIC-LVs@DMAPs in an aqueous medium (PBS pH 7.4) [61]. For this, they were placed into a 12-well plate filled with 5 mL of medium at a temperature of 37 °C. Samples of 200 μL were collected at prefixed time points (5, 10, 15, 20, 30, 40, 50, 60, and 90 min), replacing the volume sample with an equal volume of pre-warmed medium [62]. These samples were incubated with 0.1 mL of methanol to induce BIC-LVs disruption and drug solubilization. The released amount of drug was quantified by the analytical method described in section 2.14. Then, the released cumulative amounts of BIC versus time were calculated. The total drug amount released was calculated according to the previous determination of the drug content and was plotted versus time. The release profiles were fitted to the Korsmeyer-Peppas model since it considers the passive diffusion and polymer relaxation as possible

release mechanisms. In this model, low values of the exponent parameter ($n < 0.5$) denote that the release process occurs by polymer diffusion/dissolution; high values ($n > 0.85$) denote that the process is mainly governed by relaxation/swelling, whereas intermediate values ($0.5 < n < 0.85$) indicate the coexistence of both phenomena [63]. The possible burst effect was evaluated using the modification proposed by Kim [64]. Both kinetic models are described in Eqs. (3) and (4), respectively.

$$\frac{Mt}{M\infty} = k \cdot t^n \tag{3}$$

$$\frac{Mt}{M\infty} = k \cdot t^n + b \tag{4}$$

where $Mt$ is the amount released at time $t$, $M_\infty$ is the maximum amount of drug released, $Mt/M_\infty$ is the drug fraction released at time $t$, $k$ is the constant that stands for the release speed, $n$ is the release exponent that explains the mechanism that governs the process, and $b$ is the parameter associated to an initial burst effect. Finally, Higuchi model was also used as representative of pure diffusion mechanism model Eq. (5) [65].

$$\frac{Mt}{M\infty} = k \cdot \sqrt{t} \tag{5}$$

where $Mt$ is the amount released at time $t$, $M_\infty$ is the maximum amount of drug released, $Mt/ M_\infty$ is the drug fraction released at time $t$, $k$ is the constant that governs the process. Akaike information criterion (AIC) was calculated to determine the optimal model to explain the experimental data, and the correlation coefficient ($r^2$) was reported as an indicator of the proportion of variation of the results that can be explained by the model [66]. The reported results were obtained as an average of four replicates ($n = 4$).

### 2.12. In vitro biocompatibility test

*In vitro* biocompatibility of BIC-LVs@DMAPs was investigated to determine their biocompatibility in HaCaT keratinocytes [67]. For cell culture, cells were maintained in DMEM medium supplemented with 10 % fetal bovine serum (FBS), penicillin (100 IU/mL), and streptomycin (100 μg/mL) under a humidified atmosphere of 5 % $CO_2$ at a temperature of 37 °C. The cell viability was investigated by the MTT assay. For that, a suspension of cells at a density of $3{\cdot}10^6$ cells/mL was seeded onto a 96-well plate (200 μL/well) in DMEM medium supplemented with 10 % FBS, penicillin (100 IU/mL), and streptomycin (100 μg/mL). After incubation for 24 h, the medium was replaced with the same volume of DMEM medium supplemented with 0.5 % FBS and exposed for 24 h to each formulation under study at different concentrations. Then, the medium was discarded and 100 μL of MTT solution (0.5 mg/mL) was added. The supernatant was discarded after 1 h and blue deposits of colored metabolites were dissolved in 200 μL of DMSO. Absorbance at 510 nm was measured using a (VICTOR3 Multilabel Plate Reader; PerkinElmer). Results are shown as percentage of cell viability in comparison to untreated control cells Eq. (6). Percentages above 70 % were considered non-toxic, whereas those below 70 % were considered cytotoxic.

$$Cell\ viability(\%) = \frac{Absorbance\ sample}{Absorbance\ control} \cdot 100 \tag{6}$$

where absorbance sample is the absorbance of cells treated with the formulations, and absorbance control is the absorbance of non-treated cells at 510 nm.

### 2.13. Ex vivo skin drug retention and permeability studies

BIC skin retention and permeability achieved by BIC-LVs@DMAPs were evaluated in a well-established Franz-diffusion cell (FDC) setup using full-thickness mice skin [68,69]. In order to follow the three Rs principles and reduce the number of animals in *in vivo* experimentation, the mice skin was obtained from animals used in other experiments without any impact on the skin state (ethical procedure code 2021-VSC-PEA-0182). The skin was carefully shaved, excised, separated from the hypodermic tissue using a scalpel, and placed onto a foam surface covered with aluminum foil. The FDC-donor chamber was strongly attached to the skin using a small amount of cyanoacrylate glue (Loctite®). One BIC-LVs@DMAPs device was inserted into the skin using a syringe plunger to apply firm thumb-force pressure for 30 s. To secure the insertion of the BIC-LVs@DMAPs, the patches were affixed with adhesive bands (Steri-Strip®). The receptor chamber was filled with ethanol:PBS pH 7.4 (12 mL, 45:55) as described previously ($n = 5$) [70]. Temperature was maintained at 32 ± 1 °C throughout the whole experiment. The donor compartment and the sampling port were covered with Parafilm M® to avoid leakage and solvent evaporation. Samples of 200 μL were collected at prefixed times within 1.5–32.5 h. At each sampling time, the volume taken was replaced with pre-warmed ethanol:PBS pH 7.4 (45:55) to guarantee sink conditions. To determine the drug retention in the skin structure, BIC-LV@DMAPs were removed from the skin at 3, 16, 24 and 48 h. Then the skin was rinsed with PBS pH 7.4, cut in small pieces, and immersed in 5 mL of methanol overnight to extract the drug. The extracted and permeated BIC was quantified by the analytical method described in section 2.14, and the cumulative amounts of BIC were plotted versus time. Permeability parameters were calculated by linear regression of the steady state −Jmax (μg/cm$^2$h), Kp (cm/h) and tL (h)- as a simplification of the Scheuplein diffusion model. For comparative purposes, a 0.1 % (w/v) ethanolic solution (ethanol:water:propylene glycol; 60:15:25) was used as a reference, as it represents a typical topical formulation for other anti-androgenic drugs. Permeability parameters were calculated by linear regression of the steady state −Jmax (μg/cm$^2$h), Kp (cm/h) and tL (h)- as a simplification of the Scheuplein diffusion model.

### 2.14. BIC analytical detection and quantification by HPLC

BIC was quantified by High-Performance Liquid Chromatography (HPLC) using an Agilent 1260 Infinity II equipment, equipped with a UV detector settled at 272 nm, and a Kromasil® C18 column (5 μm particle size, pore size 100 Å, L × I.D. 150 mm × 4.6 mm) as stationary phase. The volume injection was 80 μL, and the mobile phase was delivered at a flow rate of 1 mL/min as an elution gradient: 1) water (0–3 min), 2) acetonitrile:phosphate buffer pH 3.0 (5:95; 3–4.5 min), 3) methanol: acetonitrile:phosphate buffer pH 3.0 (85:5:10; 4.5–8 min); followed by a washing and stabilisation phase: 4) methanol:acetonitrile (95:5; 8–11 min), 5) methanol:water (50:50; 11–14 min). BIC retention time was 6.3 min, and the total run time was 14 min. For the validation of the method, nine standard solutions in the range from 10 to 0.039 μg/mL were prepared. According to the ICH guidelines, the HPLC method was validated within the above-mentioned concentration range for inter- and intra-assay linearity, precision, sensitivity, specificity, accuracy, detection, and quantification limits [71]. Variation coefficients and relative errors remained below 5 % in all cases. Analyses were performed in triplicate ($n = 3$).

### 2.15. Statistical analysis

All data processing was performed using Microsoft Excel 2016® (Microsoft; USA) and SPSS version 22.0® (IBM Corp.; USA). Data was expressed as the mean ± standard deviation (SD) unless otherwise stated. Statistical analysis was carried out using the T-test for simple comparisons and one-way ANOVA for multiple comparisons. ANOVA tests were followed by the proper Tukey post-hoc test. Statistical differences were considered significant if p-values were below 5 % ($p < 0.05$).

## 3. Results and discussion

### 3.1. BIC-LVs production and characterization

BIC-LVs were successfully produced using Bangham's method and a milky homogeneous dispersion of nanoparticles was obtained (Fig. 1A). The opacity and pigmentation of bulk dispersions highly depend on the presence and size of the colloidal components. In this case, the white color and opacity ensured the presence of LVs. The particle size determined by Dynamic Light Scattering (DLS) showed that BIC-LVs were in the nanosized range, around 147 ± 7 nm, with an optimal PDI of 0.17 ± 0.10 (Fig. 1B). It has been previously reported that PDI values <0.3 are indicative of homogeneous particle populations for dermal and transdermal purposes [72]. Besides, 300 nm is also considered the cut-off value predictive of enhanced transdermal delivery using this type of nanoparticle [40]. Although in this study the drug delivery was mainly assisted by DMAPs, these LVs also improve the dermal penetration of BIC. Moreover, these results are in accordance with other studies that used for dermal purposes LVs with a size and PDI below 150 nm and 0.3, respectively [73,74]. Regarding the surface charge zeta potential results of BIC-LVs, a value of −24.8 ± 6.1 mV was obtained. This result is satisfactory, as it has been observed that negatively charged particles are generally less toxic to cells [75]. Additionally, the more negative (or positive) the charge, the greater the stability. Specifically, values around −30 mV are indicative of long-term colloidal stability [76]. In addition, no differences were observed between BIC-loaded particles (BIC-LVs) and Blank-LVs in terms of size, PDI and zeta potential ($p > 0.05$) (Fig. 1B). The visualization of BIC-LVs by Transmission Electron Microscopy (TEM) confirmed the size and homogeneity observations, as the estimated size was consistent, with no signs of heterogeneity

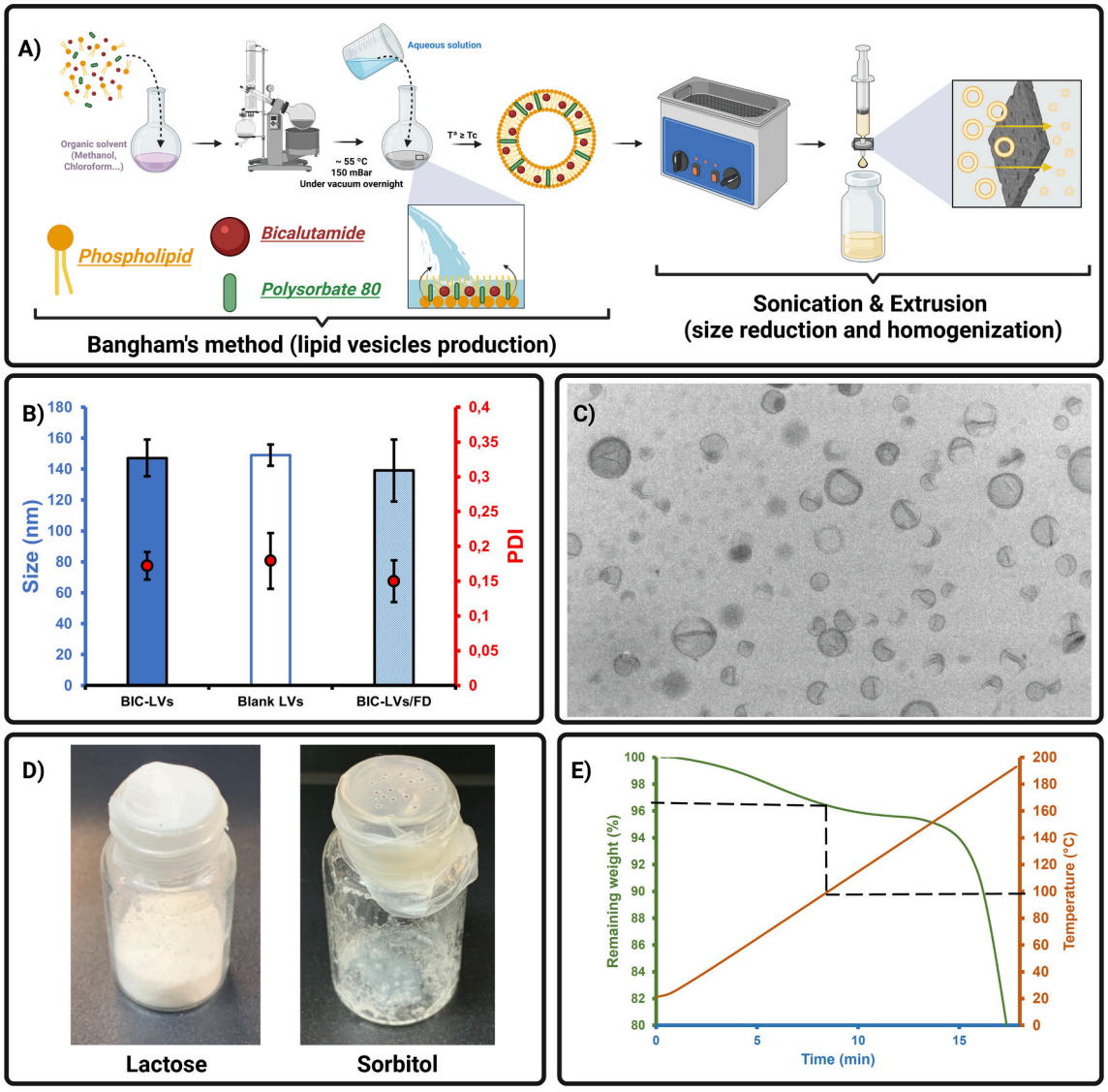


**Fig. 1. A)** Illustration of Bicalutamide (BIC)-loaded lipid vesicles (Bangham's method) and size reduction and population homogenization by sonication and extrusion. Briefly, phosphatidylcholine is dissolved with edge-activators (polysorbate 80) and drugs (BIC) in an organic solvent, which is removed in a rotary evaporator to produce a thin lipid film in the round-bottom flask. Then, the lipid thin-film is rehydrated with an aqueous solution warmed above the lipid transition temperature to produce the lipid vesicles. **B)** Size and PDI values of BIC-loaded lipid vesicles (BIC-LVs), blank lipid vesicles (Blank-LVs) and freeze-dried Bicalutamide-loaded lipid vesicles after reconstitution (BIC-LVs/FD). No differences were observed between them ($p > 0.05$). **C)** Transmission Electron Microscopy (TEM) image of BIC-LVs. **D)** Freeze-dried Bicalutamide-loaded lipid vesicles using lactose (left) and sorbitol (right) images. The use of lactose as a cryoprotectant led to a uniform and optimal product that was easily dispersible in water. Sorbitol led to a collapsed cake with suboptimal properties. **E)** Thermogravimetric analysis of the lactose-protected BIC-LVs. Water removal achieved at 100 °C represents the moisture content (around 3 %), which in this case remains below 5 %, generally accepted as a cut-off limit for freeze-dried products.

(Fig. 1C). The phospholipid determination in the assayed samples confirmed the success of the production and purification processes, as evidenced by a phospholipid recovery of 90 ± 9.2 % and minimal material loss due to manufacturing [70].

Entrapment efficiency (EE) is a critical factor for nanosized particles intended for transdermal or dermal applications, as their diffusion through the skin depends significantly on nanoparticle-driven transport and concentration gradients. Therefore, the amount of drug entrapped or encapsulated within the nanosystem plays a crucial role in drug permeation through the skin. In this sense, the EE percentage of BIC obtained from BIC-LVs was 68.9 ± 8 %, which meets EE rates obtained in other studies where lipophilic drugs were encapsulated in liposome-related vesicles [77,78]. The hydrophobic nature of this molecule facilitates the encapsulation process [79], as minimal drug loss occurs upon contact with the aqueous medium during lipid thin-film hydration. This is because the drug remains insoluble in water, with the lipid bilayer of LVs serving as its only favorable environment [40,79,80]. This high EE allowed for sufficient drug loading in the final formulation resulting in effective drug retention within the skin structure, as further reported. Freeze-drying was done as an intermediate step for preservation purposes of BIC-LVs prior to their incorporation in DMAPs. This water-removal process also avoids drug leakage and lipid oxidation during storage [81,82]. When the optimal cryoprotectant in a specific molar ratio was included, it enabled the preservation of the vesicle's structure and content. Macroscopic inspection of obtained powders denoted that the use of sorbitol led to a collapsed cake (Fig. 1D). This collapse process could imply only minor or aesthetic irregularities. However, when it occurs, the freeze-dried products are considered non-optimal [52,83]. Conversely, a uniform product with no evidence of damage was obtained when lactose was used as a cryoprotectant (Fig. 1D). Re-analysis of the samples by DLS confirmed that lactose allowed the maintenance of the size and PDI without significant changes, with results of 149 ± 6.8 nm and 0.18 ± 0.1, respectively ($p > 0.05$) (Fig. 1B). EE of BIC was also evaluated both before and after the freeze-drying process, with no significant differences observed ($p > 0.05$). Regarding surface charge, a significant decrease was observed with a measured zeta potential value of −9.5 ± 0.4 mV, probably because of the presence of cryoprotectants in the sample. However, after sorbitol use, an increase in these parameters was observed (size > 350 nm and PDI > 0.7), showing again that it was not an optimal cryoprotectant for this purpose [84]. The reason could be related to their glass transition temperatures (Tg') of maximally freeze-concentrated solution. As reported in literature, lactose and sorbitol Tg' are −28 °C and −43 °C, respectively [85]. Collapse can occur when the product temperature exceeds Tg' during sublimation, due to pressure reduction, or when it surpasses the collapse temperature (Tc) during early secondary drying [83]. However, since Tc values of both are similar, collapse most likely occurred during primary drying. These data suggest that the issue with sorbitol-containing samples likely resulted from the freeze-drying equipment failing to maintain a sufficiently low temperature during primary drying. The default setting of −50 °C, just below the Tg' of sorbitol, did not provide a sufficient safety margin throughout the process. Before evaluating the characterization properties after BIC-LV reconstitution, the residual water content of the freeze-dried powder was assessed using thermogravimetric analysis (TGA) to verify proper drying, since a maximum water content of 3–5 % is generally acceptable for freeze-dried products [86]. Thermograms showed that after heating the freeze-dried powders at 200 °C, the weight loss at 100 °C was around 3 %, meaning that the total water in the product did not represent a higher percentage than expected (Fig. 1E). Non-use of cryoprotective agents led to a typically significant increase in size and PDI (size > 800 nm and PDI > 0.5) [87]. Therefore, the mechanical stress from the freezing process was effectively mitigated by lactose, which acted as a stabilizer for the vesicle membranes and maintained lateral spacing between the phospholipids, ensuring a homogeneous size distribution [87].

### 3.2. BIC-LVs@DMAPs production and characterization

Aqueous dispersions of different biocompatible polymers were used in combination to prepare the DMAPs prototypes. PVA (9–10 kDa) and PVP (40 kDa) were the selected polymers, as their use is widely extended for biomedical applications based on their high biocompatibility [88]. It has been previously reported that the PVP-PVA combination increases the mechanical properties of the formulation, attributed to the hydrogen-bond interactions between hydroxyl groups (−OH) of PVA and carbonyl groups (C=O) of PVP [57]. Freeze-dried LVs were included in a 5 % (w/v) proportion to the formulation after their reconstitution. Under the selected conditions, proportion and polymers, the solvent casting method produced functional DMAPs (BIC-LVs@DMAPs) (Fig. 2A). Microneedles' tip length was observed by optical microscopy (Fig. 2B1), showing a length of 451 ± 15 μm, which was not affected by the presence of LVs or lactose (Fig. 2C). Thumb-force compression led to a decrease of 8.6 ± 4.4 % in BIC-LVs@DMAPs length, which was expected based on previous studies (Fig. 2B2 and Fig. 2D) [57]. No differences were reported in comparison to Blank-DMAPs and lactose-loaded DMAPs ($p > 0.05$), confirming again that the presence of BIC-LVs or lactose does not affect the physical properties of DMAPs. As observed in a representative scanning electron microscope (SEM) image of BIC-LVs@DMAPs (Fig. 2E), DMAPs exhibit sharp needle tips that can drill the outer skin layers.

Before testing the insertion and mechanical strength, a TGA analysis was performed to ensure that the drying step in the solvent casting procedure was completely concluded and final interactions between polymer–polymer and polymer-BIC-LVs were achieved. On one side, it can be considered that water removal is fully achieved after 1-week storage since 1.3 % residual water content (Fig. 2F) did not experience significant changes when compared to 2-month-old BIC-LVs@DMAPs (Fig. 2G). On the other side, it should be noted that the formulation showed high thermal stability since less than 10 % of weight mass loss was reported at 200 °C due to the polymer melting, as previously reported for PVA-based DMAPs [89]. The insertion properties of the developed BIC-LVs@DMAPs were assessed by a well-established artificial skin model to characterize microneedle devices. As observed in Fig. 2H, BIC-LVs@DMAPs were able to reach a 381 μm depth [90], although only 50 % of needle tips in the arrays reached this depth. However, nearly all needle tips penetrated to a depth of 254 μm, which is substantially greater than the approximate 50 μm thickness of the *stratum corneum* [91]. It is noteworthy that the insertion performance was not significantly affected by the presence of lactose or freeze-dried LVs. Although the insertion performance was lower, no significant differences were observed compared to blank PVA-PVP-based DMAPs ($p > 0.05$). Similar trends were observed regarding the mechanical properties.

*In vitro* release studies are regularly used in the development of pharmaceutical forms for a better understanding of the further *ex vivo* and *in vivo* performance of the formulations. These tests are enormously useful in the optimization process to make the ideal pharmaceutical product and unraveling the mechanistic behind the release process. As showed in Fig. 2I, BIC-LVs@DMAPs deliver BIC in a controlled manner. Complete drug release was achieved after 1.5 h. Nonetheless, this release process will probably be longer under *in vivo* conditions where the volume of the interstitial fluids in contact with BIC-LV@DMAPs is considerably lower. This result represents a huge advantage compared to other topically applied formulations, such as ethanolic solutions that represent the diffusion of a drug without a release or solubilization step. The kinetic modeling showed that the Korsmeyer-Peppas model fitted the data most adequately, based on the low Akaike Information Criterion (AIC) value obtained (Table 1). Besides, the correlation coefficient associated ($r^2 > 0.9$) evidenced that the model accounts for more than 90 % of the experimental variation, confirming the optimal fitting of the data to the model [66]. The Korsmeyer-Peppas model accounts for both diffusion and the relaxation or erosion of the formulation as potential

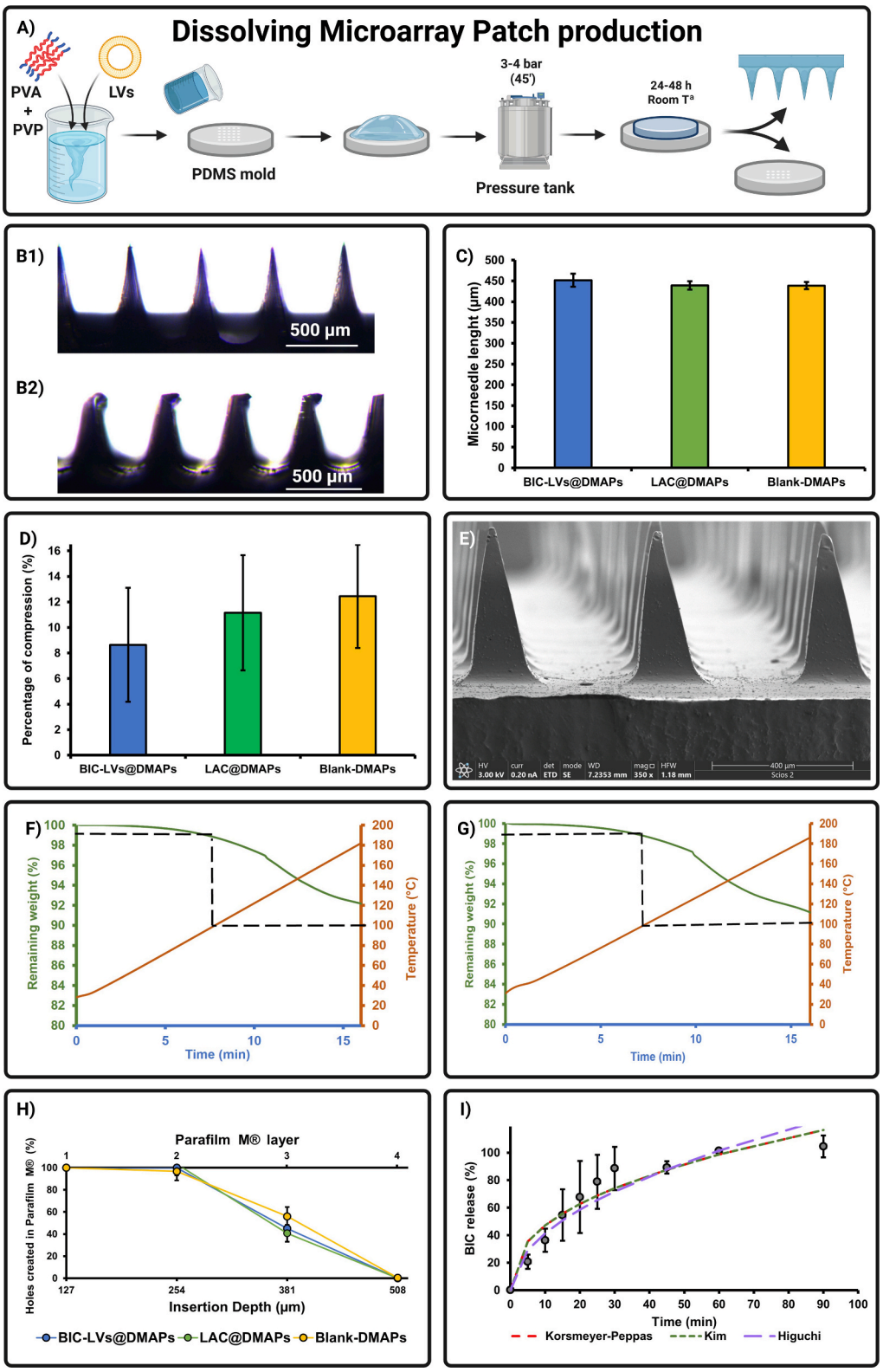


**Fig. 2.** **A)** Illustration of BIC-LVs@DMAPs production. Briefly, BIC-LVs/FD, PVP and PVA are mixed at desired concentrations and poured onto PDMS molds. Positive pressure is applied to force the gels to get into the cavities of molds, followed by drying for 24–48 h before demolding. **B)** Optical microscopy images. B1) BIC-LV@DMAPs before compression. B2) BIC-LV@DMAPs after thumb-force compression. **C)** DMAPs' tips length. No differences were observed when BIC-LVs or lactose were included ($p > 0.05$). **D)** Scanning Electron Microscopy (SEM) image of BIC-LVs@DMAPs. **E)** Thermogravimetric analysis of BIC-LVs@DMAPs after production. **F)** Thermogravimetric analysis of BIC-LVs@DMAPs after 2-month storage. No significant differences were observed when compared to E) ($p > 0.05$). **G)** Insertion properties of DMAPs in an artificial skin model. The penetration rates obtained ensured an insertion depth higher than *stratum* corneum thickness (around 50 µm). No differences were observed when BIC-LVs or lactose were included in the formulation ($p > 0.05$). **H)** Length reduction of DMAP tips after compression. No differences were observed when BIC-LVs or lactose were included in the formulation ($p > 0.05$). **I)** BIC release profile from BIC-LVs@DMAPs and kinetic model fitting (Korsmeyer-Peppas, Kim and Higuchi models).

**Table 1**
BIC-LVs@DMAPs release parameters obtained from the different kinetic models. All results are expressed as mean ± SD (n = 4).

| | k | b | n | AIC |
|---|---|---|---|---|
| **Korsmeyer-Peppas** | 19.0 ± 9.2 | – | 0.42 ± 0.12 | 74.1 ± 4.9 |
| **Kim** | 19.0 ± 9.2 | 0 | 0.42 ± 0.12 | 76.1 ± 4.9 |
| **Higuchi** | 13.1 ± 1.7 | – | – | 75.3 ± 6.5 |

release or dissolution mechanisms. It implies evident advantages over the other models, which only consider diffusion as a possible mechanism, such as the Higuchi model. The release exponent (*n*) shows that the release process from BIC-LVs@DMAPs is carried out by polymer diffusion since its value was 0.42 ± 0.12. However, relaxation cannot be completely discarded, since that value is close to 0.5, which is indicative of a double or mixed release mechanism (Table 1) [63,92].

### 3.3. *In vitro biocompatibility test*

As a consequence of their excellent biocompatibility and fusion ability with skin and cell lipids, lipid-based nanocarriers are excellent formulations to enhance transdermal drug delivery [93]. In fact, they have shown better biocompatibility than the equivalent drug solutions in certain cases [94]. For its part, the *in vivo* compatibility of PVP and PVA polymers used to fabricate DMAPs has been extensively proved. The biocompatibility of the different components of BIC-LVs@DMAPs was tested in HaCaT keratinocytes, as they are the primary cell type found in the epidermis where DMAPs are inserted (Fig. 3A).

As observed in Fig. 3B, BIC-LVs@DMAPs components were biocompatible with keratinocytes, since cell viability percentage remained above 70 % in almost all cases. Only BIC, BIC-LVs and Blank-LVs at initial concentrations after preparation were found toxic. However, the delivered doses in BIC-LV@DMAPs are considerably lower, ensuring the safety profiles at a 0.4 mg/mL concentration for both loaded and unloaded nanocarriers.

### 3.4. *Ex vivo performance of BIC-LVs@DMAPs*

*In vitro* and *ex vivo* diffusive models are an important tool to screen, study and predict the penetration ability of active ingredients in various formulations. In fact, regulatory agencies such as the FDA, approve their use to perform bioequivalence studies within the framework of topical pharmaceutical formulations and generic drugs development. Specifically, Franz-diffusion cell (FDC) is widely considered as the reference setup of these diffusive models [95]. However, systemic drug levels from a topically applied drug cannot be totally estimated using skin penetration parameters obtained *ex vivo* due to the absence of key physiological mechanisms present *in vivo* such as skin metabolism, microcirculation, and immune cell interactions. The case study in this study is consistently compatible with the FDC surrogate method since the BIC-LV@DMAPs device is intended to treat local skin conditions, such as androgenetic alopecia. This is particularly relevant in its early stages, where areas with miniaturized hair can be covered by BIC-LV@DMAPs devices. The therapeutic success of BIC and other antiandrogen drugs mainly depends on the drug concentration levels that

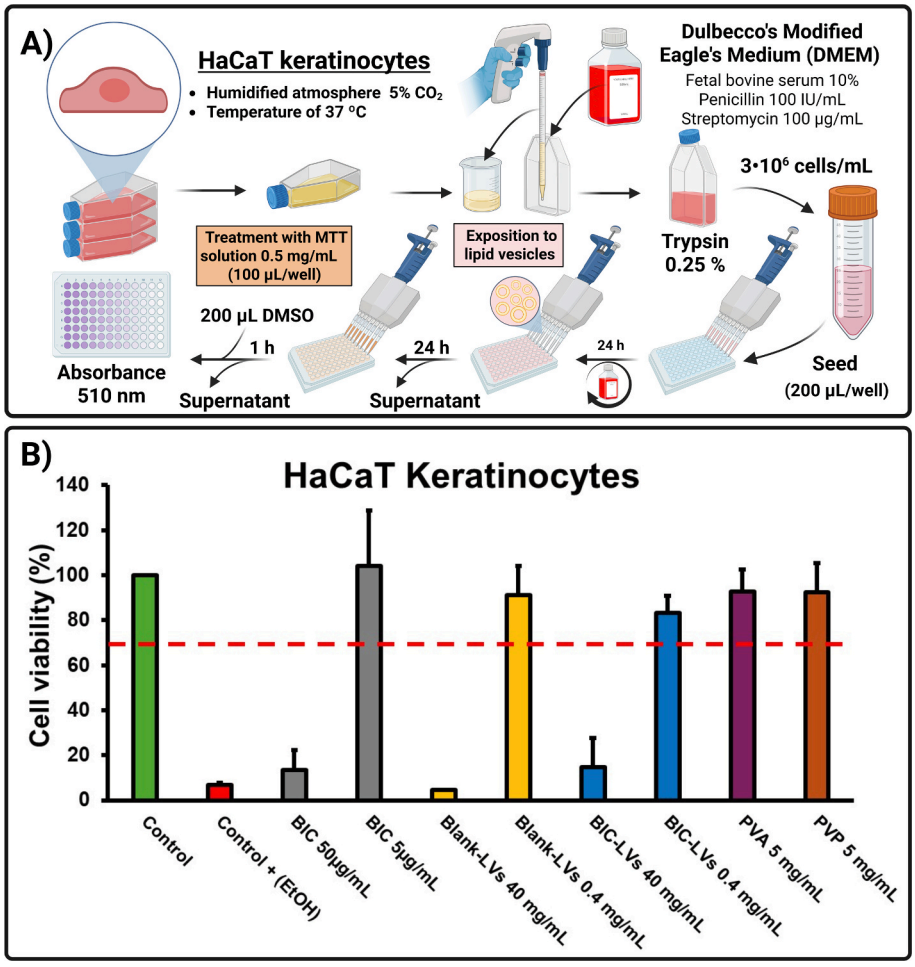


**Fig. 3. A)** Illustration of *in vitro* biocompatibility test. Percentages above 70 % were considered non-toxic, whereas those below 70 % were considered cytotoxic. **B)** HaCaT cell viability after 24 h of treatment with BIC-LVs@DMAPs components.

penetrate along the skin structure where they exert their pharmacological action, and the time that these levels are maintained. In this sense, FDC allow for the monitoring of both features. Specifically, the analytical determination of drug cumulative amounts in the receptor media over time informs about the capacity of the formulation to deliver the drug in the deeper skin strata. In addition, the BIC extraction from skin explants at different timepoints shows the drug retention within the full skin structure and not only the amounts that reached the deep skin structure.

Cumulative amounts of BIC per diffusional area of mice skin versus time and the permeability parameters calculated for BIC-LVs@DMAPs and BIC ethanolic solution 0.1 % (w/v) are presented in Fig. 4A and Table 2. The physicochemical properties of BIC predict a limited passive skin absorption, mainly because of its medium–high molecular weight and notably hydrophobic behavior. In this sense, the use of a permeability enhancer seems highly recommendable. Ethanol was selected as the solvent to solubilize BIC, a poorly water-soluble drug. However, it is well known that applying >30 % ethanol to the skin reduces skin permeability, primarily due to skin dehydration. It was observed that both systems provide effective BIC skin absorption. As observed in Fig. 4B, the BIC flux through the skin provided by the ethanolic solution was slightly higher in comparison to BIC-LVs@DMAPs. However, no significant differences can be established based on the calculated fluxes (Jmax) ($p > 0.05$) (Table 2). A similar trend was observed for lag time results. Although DMAPs needed more time to deliver the drug and reach the steady state due to a controlled BIC absorption, no significant differences were obtained in comparison to the free-BIC solution ($p > 0.05$). The reasons that can explain these findings are, on one hand, that free-BIC ethanolic solution does not present any release process that implies a delay in BIC penetration and, on the other hand, although BIC is deeply delivered into the skin structure when using DMAPs, they do not release their cargo instantly. Besides, the presence of BIC-LVs also allows a more controlled release compared to the freely available BIC in the solution. In addition, this *ex vivo* release process probably takes longer when compared to the *in vitro* drug release studies, as expected. The advantage of DMAPs over the reference solution becomes more evident when BIC doses in the formulation are considered, and permeability constants (Kp) are determined. A significant improvement was found for BIC-LVs@DMAPs since a 3-fold Kp was obtained in comparison to the ethanolic solution ($p < 0.05$). In addition, it should be noticed that these differences can be higher when translated to human skin since it has been previously reported that mice skin is strongly affected by *stratum corneum* overhydration after long or excessive exposure to liquid drug solutions [68].

**Table 2**
*Ex vivo* permeability parameters of BIC from 0.1 % (w/v) ethanolic solution and BIC-LVs@DMAPs. All results are expressed as mean ± SD (n = 5).

| | Jmax (μg/cm$^2$ h) | Kp ·10$^6$ (cm/s) | Lag time (h) |
|---|---|---|---|
| **BIC 0.1 % (w/v)** | 3.0 ± 1.1 | 1.66 ± 0.61 | 4.32 ± 1.3 |
| **BIC-LVs@DMAPs** | 1.9 ± 0.2 | 5.26 ± 0.63 | 5.18 ± 2.4 |

BIC skin retention results (Fig. 4C) revealed that BIC-LVs@DMAPs provide a controlled release delivery, as the observed BIC amounts retained in the skin increase progressively over time. Also, it should be highlighted that 40 % of the applied BIC dose from BIC-LVs@DMAPs remains in the skin structure after 48 h, which is highly interesting for the treatment of local skin conditions. On the contrary, although free-BIC ethanolic solution provided the highest flux in the permeability study, BIC skin retention was poor and erratic in comparison with BIC-LVs@DMAPs. The differences between replicates, and thus the associated variability, were considerably higher for the free-BIC ethanolic solution, where BIC concentrations in the skin remained stable only after 24 h, reaching a maximum value of 16 % of the BIC dose.

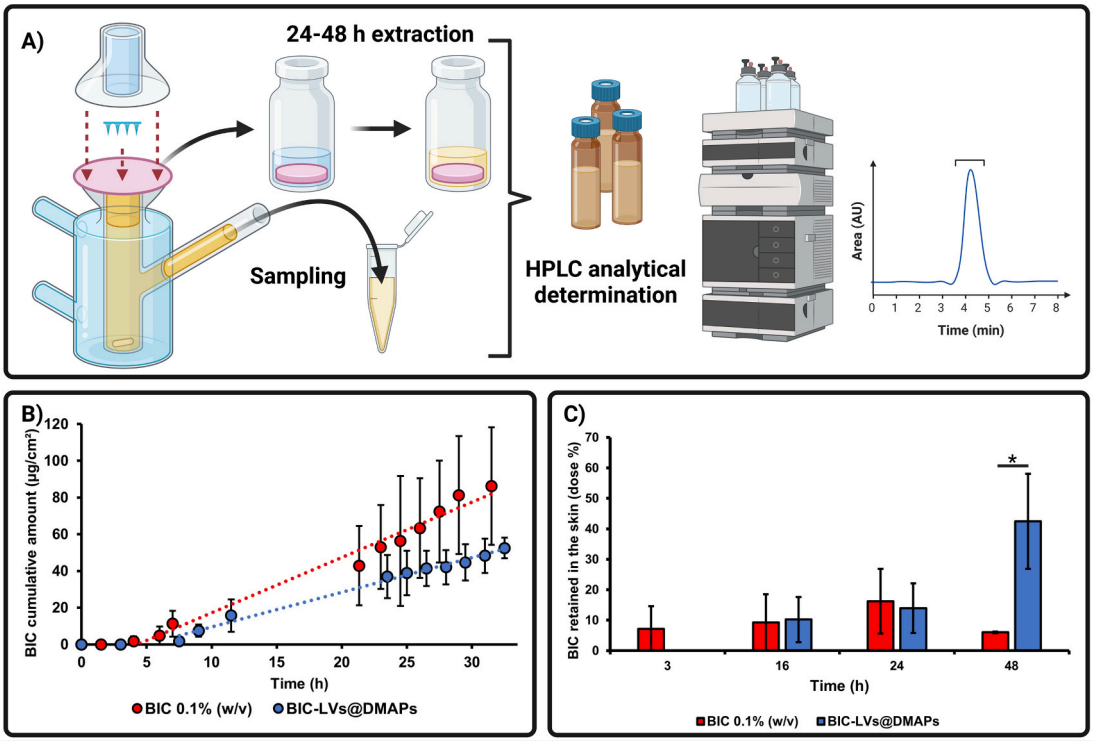


**Fig. 4. A)** Illustration of *ex vivo* penetration studies. Briefly, BIC-LVs@DMAPs were inserted into the skin and samples were taken from the receptor chamber of the Franz-diffusion cell setup. BIC retained in the skin structure was also determined after 24 and 48 h. Samples were analyzed by an HPLC analytical method. **B)** *Ex vivo* permeability profiles of BIC delivered from BIC 0.1 % (w/v) ethanolic solution (red) and BIC-LVs@DMAPs (blue). **C)** *Ex vivo* penetration amounts of BIC delivered from BIC 0.1 % (w/v) ethanolic solution (red) and BIC-LVs@DMAPs (blue) after 3, 16, 24 and 48 h. * denotes significant statistical differences. (For interpretation of the references to color in this figure legend, the reader is referred to the web version of this article.)

## 4. Conclusion

Based on the results here presented, the BIC-LVs@DMAPs strategy is a reliable approach to deliver antiandrogenic drugs for dermal purposes. Although BIC-LVs were mainly intended for allowing BIC incorporation in DMAPs, they also exhibited optimal characterization properties predictive of enhanced dermal drug delivery. PVA/PVP-based BIC-LVs@DMAPs exhibited optimal mechanical properties to effectively pierce the skin layers and assist BIC-LVs penetration to the deeper skin layers. *In vitro* biocompatibility of the formulation guaranteed its safe use. Finally, *ex vivo* studies demonstrated that BIC can be successfully delivered to the deep dermal layers, making BIC-LVs@DMAPs a promising strategy for improving the treatment of androgen-dependent skin conditions, such as androgenetic alopecia, particularly in its early stages when BIC-LVs@DMAPs devices can target areas with miniaturized hair.

## CRediT authorship contribution statement

**Miquel Martínez-Navarrete:** Writing – original draft, Visualization, Software, Methodology, Investigation, Formal analysis, Data curation, Conceptualization. **Mafalda Correia:** Writing – review & editing, Software, Methodology, Investigation, Formal analysis. **J.Alejandro Bernabeu-Martínez:** Writing – review & editing, Methodology, Investigation, Formal analysis. **Ana Cláudia Paiva-Santos:** Writing – review & editing. **Ana Borrego-Sánchez:** Writing – review & editing, Conceptualization. **Antonio José Guillot:** Writing – review & editing, Visualization, Validation, Supervision, Software, Resources, Project administration, Methodology, Funding acquisition, Formal analysis, Conceptualization.

## Funding

This publication has been economically supported by UVEG Research Funds and the "Margarita Salas" grant (ref: MS21-126) funded by the Spanish Ministry of Universities and European Union (Next generation-EU).

## Declaration of competing interest

The authors declare that they have no known competing financial interests or personal relationships that could have appeared to influence the work reported in this paper.

## Acknowledgements

Miquel Martínez-Navarrete acknowledges the financial support from ACIF grant funded by Generalitat Valenciana; Conselleria d'Innovació, Universitats, Ciència i Societat Digital (ref: CIACIF/2022/341). The authors acknowledge the logistical support provided by Prof. Ana Melero. Graphical Abstract and Illustrations were made under Biorender active license.

## Data availability

Data will be made available on request.

## References

[1] C. Lanz, M. Bennamoun, P. Macek, X. Cathelineau, R. Sanchez-Salas, The importance of antiandrogen in prostate cancer treatment, Ann. Transl. Med. 7 (2019) S362, https://doi.org/10.21037/atm.2019.09.53.
[2] T.M. Nicholson, W.A. Ricke, Androgens and estrogens in benign prostatic hyperplasia: past, present and future, Differ. Res. Biol. Divers. 82 (2011) 184–199, https://doi.org/10.1016/j.diff.2011.04.006.
[3] M. Schoelwer, E.A. Eugster, Treatment of peripheral precocious puberty, Endocr. Dev. 29 (2016) 230–239, https://doi.org/10.1159/000438895.
[4] R. Sinclair, M. Wewerinke, D. Jolley, Treatment of female pattern hair loss with oral antiandrogens, Br. J. Dermatol. 152 (2005) 466–473, https://doi.org/10.1111/j.1365-2133.2005.06218.x.
[5] P. Santhosh, M. George, Clascoterone: a new topical anti-androgen for acne management, Int. J. Dermatol. 60 (2021) 1561–1565, https://doi.org/10.1111/ijd.15752.
[6] G.E. Ryan, S. Malik, P.L. Mellon, Antiandrogen treatment ameliorates reproductive and metabolic phenotypes in the letrozole-induced mouse model of PCOS, Endocrinology 159 (2018) 1734–1747, https://doi.org/10.1210/en.2017-03218.
[7] R.S. Rittmaster, Antiandrogen treatment of polycystic ovary syndrome, Endocrinol. Metab. Clin. North Am. 28 (1999) 409–421, https://doi.org/10.1016/s0889-8529(05)70077-3.
[8] E. Ziółkowska, M. Zarzycka, T. Wiśniewski, A. Zyromska, The side effects of hormonal therapy at the patients with prostate cancer, Contemp. Oncol. (Pozn) 16 (2012) 491–497, https://doi.org/10.5114/wo.2012.32478.
[9] C. Nguyen, D.R. Lairson, M.D. Swartz, X.L. Du, Risks of major long-term side effects associated with androgen-deprivation therapy in men with prostate cancer, Pharmacotherapy 38 (2018) 999–1009, https://doi.org/10.1002/phar.2168.
[10] S.L. Mumford, A.Z. Steiner, A.Z. Pollack, N.J. Perkins, A.C. Filiberto, P.S. Albert, D. R. Mattison, J. Wactawski-Wende, E.F. Schisterman, The utility of menstrual cycle length as an indicator of cumulative hormonal exposure, J. Clin. Endocrinol. Metab. 97 (2012) E1871–E1879, https://doi.org/10.1210/jc.2012-1350.
[11] L. Wang, B. Lu, M. He, Y. Wang, Z. Wang, L. Du, Prostate cancer incidence and mortality: global status and temporal trends in 89 countries from 2000 to 2019, Front. Public Health 10 (2022) 811044, https://doi.org/10.3389/fpubh.2022.811044.
[12] R. Deswal, V. Narwal, A. Dang, C.S. Pundir, The prevalence of polycystic ovary syndrome: a brief systematic review, J. Hum. Reprod. Sci. 13 (2020) 261–271, https://doi.org/10.4103/jhrs.JHRS_95_18.
[13] Z. Mu, Y. Gao, K. Li, H. Liu, J. Zhang, Androgenetic alopecia among hospital staff: a study of prevalence, types and a comparison with general population in a secondary hospital in China, Clin. Cosmet. Investig. Dermatol. 14 (2021) 1387–1392, https://doi.org/10.2147/CCID.S333789.
[14] E.L. Aukerman, M. Jafferany, The psychological consequences of androgenetic alopecia: a systematic review, J. Cosmet. Dermatol. 22 (2023) 89–95, https://doi.org/10.1111/jocd.14983.
[15] J.J. Orme, L.C. Pagliaro, J.F. Quevedo, S.S. Park, B.A. Costello, Rational second-generation antiandrogen use in prostate cancer, Oncologist 27 (2022) 110–124, https://doi.org/10.1093/oncolo/oyab045.
[16] J.L. Beebe-Dimmer, J.J. Ruterbusch, L.C. Bylsma, C. Gillezeau, J. Fryzek, N. M. Schultz, S.C. Flanders, A. Barlev, E. Heath, R.G.W. Quek, Patterns of bicalutamide use in prostate cancer treatment: A U.S. Real-world analysis using the SEER-medicare database, Adv. Ther. 35 (2018) 1438–1451, https://doi.org/10.1007/s12325-018-0738-5.
[17] P. Yesudian, Serendipity in trichology, Int. J. Trichology 3 (2011) 1–2, https://doi.org/10.4103/0974-7753.82116.
[18] R. da S Libório, A.V. da Motta, H.A. Miot, P. Müller Ramos, Bicalutamide 25 mg combined with minoxidil 1 mg versus minoxidil 1 mg for female pattern hair loss: a randomized double-blind clinical trial, JAAD Int. 19 (2025) 48–55, https://doi.org/10.1016/j.jdin.2024.12.002.
[19] H. Akaza, S. Hinotsu, M. Usami, Y. Arai, H. Kanetake, S. Naito, Y. Hirao, Study Group for the Combined Androgen Blockade Therapy of Prostate Cancer, Combined androgen blockade with bicalutamide for advanced prostate cancer: long-term follow-up of a phase 3, double-blind, randomized study for survival, Cancer 115 (2009) 3437–3445, https://doi.org/10.1002/cncr.24395.
[20] S.N. Freeman, W.I. Mainwaring, B.J. Furr, A possible explanation for the peripheral selectivity of a novel non-steroidal pure antiandrogen, Casodex (ICI 176,334), Br. J. Cancer 60 (1989) 664–668, https://doi.org/10.1038/bjc.1989.336.
[21] A.J. Guillot, A.S. Cordeiro, R.F. Donnelly, M.C. Montesinos, T.M. Garrigues, A. Melero, Microneedle-based delivery: an overview of current applications and trends, Pharmaceutics 12 (2020) 569, https://doi.org/10.3390/pharmaceutics12060569.
[22] J.J. Escobar-Chávez, D. Bonilla-Martínez, M.A. Villegas-González, E. Molina-Trinidad, N. Casas-Alancaster, A.L. Revilla-Vázquez, Microneedles: a valuable physical enhancer to increase transdermal drug delivery, J. Clin. Pharmacol. 51 (2011) 964–977, https://doi.org/10.1177/0091270010378859.
[23] H.-R. Jeong, H.-S. Lee, I.-J. Choi, J.-H. Park, Considerations in the use of microneedles: pain, convenience, anxiety and safety, J. Drug Target. 25 (2017) 29–40, https://doi.org/10.1080/1061186X.2016.1200589.
[24] S.M. Pond, T.N. Tozer, First-pass elimination. Basic concepts and clinical consequences, Clin. Pharmacokinet. 9 (1984) 1–25, https://doi.org/10.2165/00003088-198409010-00001.
[25] D. Patel, R. Bertz, S. Ren, D.W. Boulton, M. Någård, A systematic review of gastric acid-reducing agent-mediated drug–drug interactions with orally administered medications, Clin. Pharmacokinet. 59 (2020) 447–462, https://doi.org/10.1007/s40262-019-00844-3.
[26] A.Y. Abuhelwa, D.B. Williams, R.N. Upton, D.J.R. Foster, Food, gastrointestinal pH, and models of oral drug absorption, Eur. J. Pharm. Biopharm. 112 (2017) 234–248, https://doi.org/10.1016/j.ejpb.2016.11.034.
[27] R.L. Parsons, Drug absorption in gastrointestinal disease with particular reference to malabsorption syndromes, Clin. Pharmacokinet. 2 (1977) 45–60, https://doi.org/10.2165/00003088-197702010-00004.
[28] B. Schutijser, J.E. Klopotowska, I. Jongerden, P. Spreeuwenberg, C. Wagner, M. de Bruijne, Nurse compliance with a protocol for safe injectable medication administration: comparison of two multicentre observational studies, BMJ Open 8 (2018) e019648, https://doi.org/10.1136/bmjopen-2017-019648.

[29] H.S. Gill, D.D. Denson, B.A. Burris, M.R. Prausnitz, Effect of microneedle design on pain in human volunteers, Clin. J. Pain 24 (2008) 585–594, https://doi.org/10.1097/AJP.0b013e31816778f9.
[30] R.F. Donnelly, M.R. Prausnitz, The promise of microneedle technologies for drug delivery, Drug Deliv. Transl. Res. 14 (2024) 573–580, https://doi.org/10.1007/s13346-023-01430-8.
[31] N.G. Oh, S.Y. Hwang, Y.H. Na, Fabrication of a PVA-based hydrogel microneedle patch, ACS Omega 7 (2022) 25179–25185, https://doi.org/10.1021/acsomega.2c01993.
[32] I.C. Lee, Y.C. Wu, S.W. Tsai, C.H. Chen, M.H. Wu, Fabrication of two-layer dissolving polyvinylpyrrolidone microneedles with different molecular weights for in vivo insulin transdermal delivery, RSC Adv. 7 (2017) 5067–5075, https://doi.org/10.1039/C6RA27476E.
[33] P.S. Castañeda, C.L. Domínguez Delgado, I.M.R. Cruz, L.M.M. Contreras, E.M. M. Trinidad, M.L. Cervantes, J.J. Escobar-Chávez, Development of poly (Methyl vinyl ether-alt-maleic acid) microneedles for transdermal delivery of atorvastatin calcium, Curr. Pharm. Biotechnol. 21 (2020) 852–861, https://doi.org/10.2174/1389201021666200217103302.
[34] I. Saha, V.K. Rai, Hyaluronic acid based microneedle array: Recent applications in drug delivery and cosmetology, Carbohydr. Polym. 267 (2021) 118168, https://doi.org/10.1016/j.carbpol.2021.118168.
[35] E.G. Yilmaz, E. Ece, Ö. Erdem, I. Eş, F. Inci, A sustainable solution to skin diseases: ecofriendly transdermal patches, Pharmaceutics 15 (2023) 579, https://doi.org/10.3390/pharmaceutics15020579.
[36] R.S.J. Ingrole, E. Azizoglu, M. Dul, J.C. Birchall, H.S. Gill, M.R. Prausnitz, Trends of microneedle technology in the scientific literature, patents, clinical trials and internet activity, Biomaterials 267 (2021) 120491, https://doi.org/10.1016/j.biomaterials.2020.120491.
[37] A.J. Guillot, M. Martínez-Navarrete, V. Zinchuk-Mironova, A. Melero, Microneedle-assisted transdermal delivery of nanoparticles: Recent insights and prospects, Wiley Interdiscip. Rev. Nanomed. Nanobiotechnol. 15 (2023) e1884, https://doi.org/10.1002/wnan.1884.
[38] T. Waghule, G. Singhvi, S.K. Dubey, M.M. Pandey, G. Gupta, M. Singh, K. Dua, Microneedles: a smart approach and increasing potential for transdermal drug delivery system, Biomed. Pharmacother. Biomedecine Pharmacother. 109 (2019) 1249–1258, https://doi.org/10.1016/j.biopha.2018.10.078.
[39] W. Li, R.N. Terry, J. Tang, M.R. Feng, S.P. Schwendeman, M.R. Prausnitz, Rapidly separable microneedle patch for the sustained release of a contraceptive, Nat. Biomed. Eng. 3 (2019) 220–229, https://doi.org/10.1038/s41551-018-0337-4.
[40] A.J. Guillot, M. Martínez-Navarrete, T.M. Garrigues, A. Melero, Skin drug delivery using lipid vesicles: a starting guideline for their development, J. Control. Release 355 (2023) 624–654, https://doi.org/10.1016/j.jconrel.2023.02.006.
[41] A.J. Guillot, E. Jornet-Mollá, N. Landsberg, C. Milián-Guimerá, M.C. Montesinos, T. M. Garrigues, A. Melero, Cyanocobalamin ultraflexible lipid vesicles: characterization and in vitro evaluation of drug-skin depth profiles, Pharmaceutics 13 (2021) 418, https://doi.org/10.3390/pharmaceutics13030418.
[42] A.J. Guillot, P. Merino, A. Bocchino, C. O'Mahony, R. Ma Giner, M. Carmen Recio, T.M. Garrigues, A. Melero, Exploration of microneedle-assisted skin delivery of cyanocobalamin formulated in ultraflexible lipid vesicles, Eur. J. Pharm. Biopharm. 177 (2022) 184–198, https://doi.org/10.1016/j.ejpb.2022.06.015.
[43] C. Théry, S. Amigorena, G. Raposo, A. Clayton, Isolation and characterization of exosomes from cell culture supernatants and biological fluids, Curr. Protoc. Cell Biol. 3 (Unit 3.22) (2006), https://doi.org/10.1002/0471143030.cb0322s30.
[44] P. Panwar, B. Pandey, P.C. Lakhera, K.P. Singh, Preparation, characterization, and in vitro release study of albendazole-encapsulated nanosize liposomes, Int. J. Nanomed. 5 (2010) 101–108, https://doi.org/10.2147/ijn.s8030.
[45] S. Keller, H. Heerklotz, N. Jahnke, A. Blume, Thermodynamics of lipid membrane solubilization by sodium dodecyl sulfate, Biophys. J. 90 (2006) 4509–4521, https://doi.org/10.1529/biophysj.105.077867.
[46] J. Hernández-Borrell, M. Pons, J.C. Juarez, J. Estelrich, The action of Triton X-100 and sodium dodecyl sulphate on lipid layers. effect on monolayers and liposomes, J. Microencapsul. 7 (1990) 255–259, https://doi.org/10.3109/02652049009021838.
[47] T. Igarashi, Y. Shoji, K. Katayama, Anomalous solubilization behavior of dimyristoylphosphatidylcholine liposomes induced by sodium dodecyl sulfate micelles, Anal. Sci. Int. J. Jpn. Soc. Anal. Chem. 28 (2012) 345–350, https://doi.org/10.2116/analsci.28.345.
[48] K. Nakano, Y. Tozuka, H. Yamamoto, Y. Kawashima, H. Takeuchi, A novel method for measuring rigidity of submicron-size liposomes with atomic force microscopy, Int. J. Pharm. 355 (2008) 203–209, https://doi.org/10.1016/j.ijpharm.2007.12.018.
[49] Z. Varga, B. Fehér, D. Kitka, A. Wacha, A. Bóta, S. Berényi, V. Pipich, J.-L. Fraikin, Size measurement of extracellular vesicles and synthetic liposomes: the impact of the hydration shell and the protein corona, Colloids Surf. B Biointerf. 192 (2020) 111053, https://doi.org/10.1016/j.colsurfb.2020.111053.
[50] I.M. Tucker, J.C.W. Corbett, J. Fatkin, R.O. Jack, M. Kaszuba, B. MacCreath, F. McNeil-Watson, Laser doppler electrophoresis applied to colloids and surfaces, Curr. Opin. Colloid Interf. Sci. 20 (2015) 215–226, https://doi.org/10.1016/j.cocis.2015.07.001.
[51] G. Rouser, S. Fleischer, A. Yamamoto, Two dimensional thin layer chromatographic separation of polar lipids and determination of phospholipids by phosphorus analysis of spots, Lipids 5 (1970) 494–496, https://doi.org/10.1007/BF02531316.
[52] S. Franzé, F. Selmin, E. Samaritani, P. Minghetti, F. Cilurzo, Lyophilization of liposomal formulations: still necessary still challenging, Pharmaceutics 10 (2018) E139, https://doi.org/10.3390/pharmaceutics10030139.
[53] B. Stark, G. Pabst, R. Prassl, Long-term stability of sterically stabilized liposomes by freezing and freeze-drying: effects of cryoprotectants on structure, Eur. J. Pharm. Sci. 41 (2010) 546–555, https://doi.org/10.1016/j.ejps.2010.08.010.
[54] J. Sabín, X. Prieto, S. Sennato, E. Blanco, P. Messina, J. Ruso, R. Angelini, F. Bordi, F. Sarmiento, Examinationof the influence of F6H10 fluorinated diblocks on DPPC liposomes, J. Therm. Anal. Calorim. 87 (2007) 301–304, https://doi.org/10.1007/s10973-006-7846-1.
[55] M. Martínez-Navarrete, A.J. Guillot, M.C. Lobita, M.C. Recio, R. Giner, J. Aparicio-Blanco, M.C. Montesinos, H.A. Santos, A. Melero, Cyclosporin A-loaded dissolving microneedles for dermatitis therapy: Development, characterisation and efficacy in a delayed-type hypersensitivity in vivo model, Drug Deliv. Transl. Res. 14 (2024) 3404–3421, https://doi.org/10.1007/s13346-024-01542-9.
[56] A.J. Guillot, M. Martínez-Navarrete, R.M. Giner, M.C. Recio, H.A. Santos, A. S. Cordeiro, A. Melero, Cyanocobalamin-loaded dissolving microneedles diminish skin inflammation in vivo, J. Control. Release 375 (2024) 537–551, https://doi.org/10.1016/j.jconrel.2024.09.032.
[57] A.D. Permana, I.A. Tekko, M.T.C. McCrudden, Q.K. Anjani, D. Ramadon, H. O. McCarthy, R.F. Donnelly, Solid lipid nanoparticle-based dissolving microneedles: A promising intradermal lymph targeting drug delivery system with potential for enhanced treatment of lymphatic filariasis, J. Controlled Release 316 (2019) 34–52, https://doi.org/10.1016/j.jconrel.2019.10.004.
[58] J.-F. Liao, J.-C. Lee, C.-K. Lin, K.-C. Wei, P.-Y. Chen, H.-W. Yang, Self-assembly DNA polyplex vaccine inside dissolving microneedles for high-potency intradermal vaccination, Theranostics 7 (2017) 2593–2605, https://doi.org/10.7150/thno.19894.
[59] R.F. Donnelly, R. Majithiya, T.R.R. Singh, D.I.J. Morrow, M.J. Garland, Y.K. Demir, K. Migalska, E. Ryan, D. Gillen, C.J. Scott, A.D. Woolfson, Design, optimization and characterisation of polymeric microneedle arrays prepared by a novel laser-based micromoulding technique, Pharm. Res. 28 (2011) 41–57, https://doi.org/10.1007/s11095-010-0169-8.
[60] E. Larrañeta, J. Moore, E.M. Vicente-Pérez, P. González-Vázquez, R. Lutton, A. D. Woolfson, R.F. Donnelly, A proposed model membrane and test method for microneedle insertion studies, Int. J. Pharm. 472 (2014) 65–73, https://doi.org/10.1016/j.ijpharm.2014.05.042.
[61] E. Larrañeta, S. Stewart, S.J. Fallows, L.L. Birkhäuer, M.T.C. McCrudden, A. D. Woolfson, R.F. Donnelly, A facile system to evaluate in vitro drug release from dissolving microneedle arrays, Int. J. Pharm. 497 (2016) 62–69, https://doi.org/10.1016/j.ijpharm.2015.11.038.
[62] D. Solomon, N. Gupta, N.S. Mulla, S. Shukla, Y.A. Guerrero, V. Gupta, Role of In vitro release methods in liposomal formulation development: challenges and regulatory perspective, AAPS J. 19 (2017) 1669–1681, https://doi.org/10.1208/s12248-017-0142-0.
[63] P.L. Ritger, N.A. Peppas, A simple equation for description of solute release II. fickian and anomalous release from swellable devices, J. Control. Release 5 (1987) 37–42, https://doi.org/10.1016/0168-3659(87)90035-6.
[64] H. Kim, R. Fassihi, Application of binary polymer system in drug release rate modulation. 2. Influence of formulation variables and hydrodynamic conditions on release kinetics, J. Pharm. Sci. 86 (1997) 323–328, https://doi.org/10.1021/js960307p.
[65] T. Higuchi, Rate of release of medicaments from ointment bases containing drugs in suspension, J. Pharm. Sci. 50 (1961) 874–875, https://doi.org/10.1002/jps.2600501018.
[66] D.F. Hamilton, M. Ghert, A.H.R.W. Simpson, Interpreting regression models in clinical outcome studies, Bone Jt. Res. 4 (2015) 152–153, https://doi.org/10.1302/2046-3758.49.2000571.
[67] J. López-García, M. Lehocký, P. Humpolíček, P. Sáha, HaCaT keratinocytes response on antimicrobial atelocollagen substrates: extent of cytotoxicity, cell viability and proliferation, J. Funct. Biomater. 5 (2014) 43–57, https://doi.org/10.3390/jfb5020043.
[68] H. Todo, Transdermal permeation of drugs in various animal species, Pharmaceutics 9 (2017) E33, https://doi.org/10.3390/pharmaceutics9030033.
[69] S.F. Ng, J.J. Rouse, F.D. Sanderson, V. Meidan, G.M. Eccleston, Validation of a static Franz diffusion cell system for in vitro permeation studies, AAPS Pharm. Sci. Tech. 11 (2010) 1432–1441, https://doi.org/10.1208/s12249-010-9522-9.
[70] J.J. Carreras, W.E. Tapia-Ramirez, A. Sala, A.J. Guillot, T.M. Garrigues, A. Melero, Ultraflexible lipid vesicles allow topical absorption of cyclosporin A, Drug Deliv. Transl. Res. 10 (2020) 486–497, https://doi.org/10.1007/s13346-019-00693-4.
[71] M. Miranda, C. Cardoso, C. Vitorino, Fast screening methods for the analysis of topical drug products, Processes 8 (2020) 397, https://doi.org/10.3390/pr8040397.
[72] M. Danaei, M. Dehghankhold, S. Ataei, F. Hasanzadeh Davarani, R. Javanmard, A. Dokhani, S. Khorasani, M.R. Mozafari, Impact of particle size and polydispersity index on the clinical applications of lipidic nanocarrier systems, Pharmaceutics 10 (2018) E57, https://doi.org/10.3390/pharmaceutics10020057.
[73] A. Ahad, A.A. Al-Saleh, A.M. Al-Mohizea, F.I. Al-Jenoobi, M. Raish, A.E.B. Yassin, M.A. Alam, Formulation and characterization of novel soft nanovesicles for enhanced transdermal delivery of eprosartan mesylate, Saudi Pharm. J. SPJ 25 (2017) 1040–1046, https://doi.org/10.1016/j.jsps.2017.01.006.
[74] A. Ahad, A.A. Al-Saleh, A.M. Al-Mohizea, F.I. Al-Jenoobi, M. Raish, A.E.B. Yassin, M.A. Alam, Formulation and characterization of Phospholipon 90 G and tween 80 based transfersomes for transdermal delivery of eprosartan mesylate, Pharm. Dev. Technol. 23 (2018) 787–793, https://doi.org/10.1080/10837450.2017.1330345.
[75] J.S. Bozich, S.E. Lohse, M.D. Torelli, C.J. Murphy, R.J. Hamers, R.D. Klaper, Surface chemistry, charge and ligand type impact the toxicity of gold nanoparticles to Daphnia magna, Environ. Sci. Nano 1 (2014) 260–270, https://doi.org/10.1039/C4EN00006D.

[76] G. Midekessa, K. Godakumara, J. Ord, J. Viil, F. Lättekivi, K. Dissanayake, S. Kopanchuk, A. Rinken, A. Andronowska, S. Bhattacharjee, T. Rinken, A. Fazeli, Zeta potential of extracellular vesicles: toward understanding the attributes that determine colloidal stability, ACS Omega 5 (2020) 16701–16710, https://doi.org/10.1021/acsomega.0c01582.

[77] R. Cortesi, E. Esposjto, G. Luca, C. Nastruzzi, Production of lipospheres as carriers for bioactive compounds, Biomaterials 23 (2002) 2283–2294, https://doi.org/10.1016/s0142-9612(01)00362-3.

[78] J.C. Villamil, C.M. Parra-Giraldo, L.D. Pérez, Enhancing the performance of PEG-b-PCL copolymers as precursors of micellar vehicles for amphotericin B through its conjugation with cholesterol, Colloids Surf. Physicochem. Eng. Asp. 572 (2019) 79–87, https://doi.org/10.1016/j.colsurfa.2019.03.086.

[79] D.L. Gbian, A. Omri, Lipid-based drug delivery systems for diseases managements, Biomedicines 10 (2022) 2137, https://doi.org/10.3390/biomedicines10092137.

[80] H. Nsairat, D. Khater, U. Sayed, F. Odeh, A. Al Bawab, W. Alshaer, Liposomes: structure, composition, types, and clinical applications, Heliyon 8 (2022) e09394, https://doi.org/10.1016/j.heliyon.2022.e09394.

[81] T. Liang, R. Guan, Z. Quan, Q. Tao, Z. Liu, Q. Hu, Cyanidin-3-o-glucoside liposome: Preparation via a green method and antioxidant activity in GES-1 cells, Food Res. Int. Ott. Ont 125 (2019) 108648, https://doi.org/10.1016/j.foodres.2019.108648.

[82] E. Schnitzer, I. Pinchuk, A. Bor, A. Leikin-Frenkel, D. Lichtenberg, Oxidation of liposomal cholesterol and its effect on phospholipid peroxidation, Chem. Phys. Lipids 146 (2007) 43–53, https://doi.org/10.1016/j.chemphyslip.2006.12.003.

[83] S.M. Patel, S.L. Nail, M.J. Pikal, R. Geidobler, G. Winter, A. Hawe, J. Davagnino, S. Rambhatla Gupta, Lyophilized drug product cake appearance: what is acceptable? J. Pharm. Sci. 106 (2017) 1706–1721, https://doi.org/10.1016/j.xphs.2017.03.014.

[84] C. Chen, D. Han, C. Cai, X. Tang, An overview of liposome lyophilization and its future potential, J. Control. Release 142 (2010) 299–311, https://doi.org/10.1016/j.jconrel.2009.10.024.

[85] A.T. Skrabanja, A.L. de Meere, R.A. de Ruiter, P.J. van den Oetelaar, Lyophilization of biotechnology products, PDA J. Pharm. Sci. Technol. 48 (1994) 311–317.

[86] A. Molnar, T. Lakat, A. Hosszu, B. Szebeni, A. Balogh, L. Orfi, A.J. Szabo, A. Fekete, J. Hodrea, Lyophilization and homogenization of biological samples improves reproducibility and reduces standard deviation in molecular biology techniques, Amino Acids 53 (2021) 917–928, https://doi.org/10.1007/s00726-021-02994-w.

[87] C.J. Garvey, T. Lenné, K.L. Koster, B. Kent, G. Bryant, Phospholipid membrane protection by sugar molecules during dehydration—insights into molecular mechanisms using scattering techniques, Int. J. Mol. Sci. 14 (2013) 8148–8163, https://doi.org/10.3390/ijms14048148.

[88] M. Teodorescu, M. Bercea, S. Morariu, Biomaterials of PVA and PVP in medical and pharmaceutical applications: perspectives and challenges, Biotechnol. Adv. 37 (2019) 109–131, https://doi.org/10.1016/j.biotechadv.2018.11.008.

[89] M.S. Arshad, S. Zafar, A.T. Zahra, M.H. Zaman, A. Akhtar, I. Kucuk, M. Farhan, M.-W. Chang, Z. Ahmad, Fabrication and characterisation of self-applicating heparin sodium microneedle patches, J. Drug Target. 29 (2021) 60–68, https://doi.org/10.1080/1061186X.2020.1795180.

[90] R.F. Donnelly, K. Moffatt, A.Z. Alkilani, E.M. Vicente-Pérez, J. Barry, M.T. C. McCrudden, A.D. Woolfson, Hydrogel-forming microneedle arrays can be effectively inserted in skin by self-application: a pilot study centred on pharmacist intervention and a patient information leaflet, Pharm. Res. 31 (2014) 1989–1999, https://doi.org/10.1007/s11095-014-1301-y.

[91] H. Dawud, A. Abu Ammar, Rapidly dissolving microneedles for the delivery of steroid-loaded nanoparticles intended for the treatment of inflammatory skin diseases, Pharmaceutics 15 (2023) 526, https://doi.org/10.3390/pharmaceutics15020526.

[92] P.L. Ritger, N.A. Peppas, A simple equation for description of solute release I. Fickian and non-fickian release from non-swellable devices in the form of slabs, spheres, cylinders or discs, J. Control. Release 5 (1987) 23–36, https://doi.org/10.1016/0168-3659(87)90034-4.

[93] M.K. Chourasia, L. Kang, S.Y. Chan, Nanosized ethosomes bearing ketoprofen for improved transdermal delivery, Results Pharma Sci. 1 (2011) 60–67, https://doi.org/10.1016/j.rinphs.2011.10.002.

[94] Y.T. Zhang, L.N. Shen, Z.H. Wu, J.H. Zhao, N.P. Feng, Comparison of ethosomes and liposomes for skin delivery of psoralen for psoriasis therapy, Int. J. Pharm. 471 (2014) 449–452, https://doi.org/10.1016/j.ijpharm.2014.06.001.

[95] M. Miranda, Z. Volmer, A. Cornick, A. Goody, C. Cardoso, A.A.C.C. Pais, M. Brown, C. Vitorino, *In vitro* studies into establishing therapeutic bioequivalence of complex topical products: Weight of evidence, Int. J. Pharm. 656 (2024) 124012, https://doi.org/10.1016/j.ijpharm.2024.124012.